

DC and quench performance assessment from the EUROfusion HTS Quench Experiment campaign and projection to magnet operation[☆]

A. Zappatore^a, H. Bajas^b, N. Bykovskiy^c, P. Bruzzone^c, G. Celentano^d, G. Colombo^e, J. Greenwood^c, A. Masi^d, K. Sedlak^c, D. Uglietti^c, V. Corato^{d,*}

^a NEMO Group, Dipartimento Energia, Politecnico di Torino, Italy

^b Formerly at Ecole Polytechnique Fédérale de Lausanne (EPFL), Swiss Plasma Center (SPC), CH-5232 Villigen PSI, Switzerland

^c Ecole Polytechnique Fédérale de Lausanne (EPFL), Swiss Plasma Center (SPC), CH-5232 Villigen PSI, Switzerland

^d Superconductivity Laboratory, Nuclear Department, ENEA, Frascati, Italy

^e Department of Electrical, Electronic and Information Engineering "Guglielmo Marconi" - DEL, University of Bologna, Italy

ABSTRACT

Seven different high current conductors for fusion applications, made of High Temperature Superconducting stacked tapes, have been successfully tested in the Quench Experiment campaign supported by EUROfusion and carried out in SULTAN. The aim of this extensive experimental campaign is to explore the quench initiation and propagation in different conditions as well as different conductor design. The measurements show that there is a common behaviour to all layouts, i.e., the DC performance of such conductors have degraded after the quench test campaign, and more systematic DC experiments showed that it is likely that a temperature peak beyond 150 K on the stack may lead to the degradation. These results are analyzed and discussed in the present work. This allowed identifying a reference threshold for the safe operation in a real magnet. Through a simple analytical model, based on the assumption of adiabatic quench propagation, the projection to the expected performance in the magnet configuration is carried out, focusing on the maximum hotspot temperature reached, depending on the layout. It is shown that conductors with a larger effective heat capacity, although having a smaller quench propagation velocity, end up having lower hotspot temperature.

1. Introduction

High temperature superconducting (HTS) materials are currently being used to build conductors and magnets relevant for fusion applications, i.e., carrying high current to generate high magnetic fields. The research and development process worldwide is targeting conductors, which are needed for pulsed magnets, as well as non-insulated magnets, which may be feasible for steady operation. Several conductor designs have been proposed and tested, such as those based on the twisted-stacked tapes approach [1,2,3] or on the CORC approach [4], while there are only few examples of (large) non-insulated magnets [5].

The necessity to use insulated conductors to wind pulsed magnets poses the problem of quench detection and protection, which is well known to be a more challenging issue with respect to conductors built with low temperature superconducting materials, mainly due to the larger margin of the high temperature counterpart. Furthermore, being a newer technology, until few years ago, there was a lack of experimental investigation of the quench behaviour at the (HTS) conductor scale.

For this reason, EUROfusion has started an experimental campaign

focused on the investigation of the quench propagation in HTS conductors, designed by different research units in the EUROfusion consortium itself, because such types of conductors are relevant for the hybrid design of the EU DEMO Central Solenoid [6]. The first being tested were those designed and manufactured by the Swiss Plasma Center (SPC) and the results were analysed in [7] and [8] in terms of quench propagation velocity (QPV) and hotspot temperature. The data were also used to calibrate and validated numerical models based on 1D [8] or 3D [9] approaches. In 2023 and 2024, conductors designed and manufactured by ENEA were also tested.

An overview of the conductor designs and their main dimensions are reported in Table 1. All the conductors are based on the stacked-tapes approach: tens of tapes are stacked together and put electrically in parallel. Each conductor features a dedicated cooling channel to allow active cooling through forced flow helium. The conductor design is based on the Cable-In-Conduit approach for all the samples. All conductors were manufactured using REBCO tapes, except for a BiSCCO conductor designed and manufactured by SPC [7]. In this work the focus is on the REBCO conductors.

[☆] This article is part of a special issue entitled: 'SPAS-2024' published in Cryogenics.

* Corresponding author.

E-mail address: valentina.corato@enea.it (V. Corato).

In this paper, after a brief description of the experiment in Section 2, a focus is given -in Section 3- on the evolution of the DC performance of the conductors tested so far, which all showed degradation after the quench test campaign. Through a simple analytical method, summarized in Section 4 and validated against the available data, the projection to the magnet-relevant conditions is presented and discussed in Section 5, allowing a thorough comparison between all the layouts tested so far.

2. Description of the experiment

The tests were carried out in SULTAN [10], which was upgraded to provide a maximum of 15 kA at 10 V. The sample is made by two 3.6 m long conductors, which are connected electrically in series through a joint (hairpin configuration) and cooled in parallel, so that they can be operated at different temperature at the same time. A background magnetic field can be provided by the facility. The portion of the conductor where the magnetic field is the largest (up to a maximum value of 10.9 T) and uniform over 40 cm is called High Field Zone (HFZ), see Fig. 1(a). Thus, the quench is expected to start propagating in this region. The conductor designs and their instrumentation are briefly recalled in the remaining part of this Section.

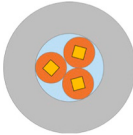
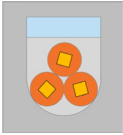


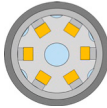
The ENEA conductors are based on the slotted-core concept presented in [2]. In these conductors, tapes are stacked, without being soldered, and placed in the slots of an aluminum core. On top of the stacks, aluminum fillers are fitted in order to provide compression on the stacks. The cable is then jacketed in an aluminum conduit, which provides containment for the helium. In the SULTAN experiment, an additional external stainless-steel 1 mm thick conduit was added. This was made for both providing additional mechanical reinforcement and ensuring helium tightness at the terminations. Also, the slots of all the tested conductors are untwisted. The aluminum conduit for all the conductors was 1.25 mm thick, while the core has an external diameter of 22.6 mm. To provide active cooling to the conductor, a central channel (7 mm in diameter) in the core is present. The coolant can also flow in the voids in the slots between the core and the stacks as well as in the small channels around the external side of the core, see the cross-section of the ENEA conductor in Fig. 1(b).

The three ENEA conductors tested differ in the following way: from the design point of view, A1 and A2 were identical, with 76 tapes inserted in 4 out of the total 6 slots and all the stacks are oriented with a tilt of 30° between the background field and the tapes c-axis, see Fig. 1 (b). In B1, all the slots were filled, each with 13 tapes. The orientation of the conductor is the same, thus 2 of the 6 stacks in B1 are oriented with the ab plane parallel to the background field. From the instrumentation point of view, in all the conductors, voltage taps were placed on the external side of the stainless steel conduit ($V_{\#}$ in Fig. 1(a)). In addition, five taps were placed in contact with the core in the HFZ, each at a distance of 10 cm from the other ($V_{\#bis}$ in Fig. 1(a)). The latter, in the HFZ, are 5 cm staggered with respect to those on the external jacket, see again Fig. 1(a). Concerning the temperature, in all the conductors it was measured on the external jacket (sensor X), but in A1 and B1 additional sensors were added protruding them through the two jackets to measure the temperature on top of two different stacks (sensor Y, labelled $T_{\#}^*$, see Fig. 1(a)). The helium temperature was also measured at different locations (sensor Z), see Fig. 1(b), through helium-tight temperature sensor protruding up to the central channel. The temperature in A2 was measured only on the external jacket.

The quench experiment is performed by heating the helium (through electric heaters on the feeding pipes) flowing in the investigated conductor (it was possible to fire the heaters independently, thus bringing to quench only one of the two conductors constituting the SULTAN sample) by monitoring the voltage and temperature evolution until the quench is triggered. The quench run is then stopped (by turning off the current) as soon as a given voltage threshold is reached. The sequence of quench tests was performed increasing this voltage threshold, in order to reach progressively larger hot-spot temperatures.

The four different REBCO conductors designed and tested by SPC are named as Reference, Solder-twisted, Solder-filled and ASTRA. The first three are made of three strands. Each strand is made by a stack of tapes (yellow squares in Table 1), which is tightly enclosed in a copper profile (orange regions in Table 1), whose outer diameter is 8.5 mm. The soldering of the stacks and the copper profiles is performed after the twisting of the strand (HTS stack + copper profiles). In the Reference and Solder-filled conductors, the strands and the triplet are twisted with

Table 1
Overview of the cross-sections of the tested conductors so far.

Conductor	Reference/Non-twisted	Solder-filled	ASTRA	ENEA A1/A2	ENEA B1
					
Stabilizer material	Copper			Aluminum	
$A_{\text{stabilizer}}$ [mm ²]	150	150	144	255	292
A_{jacket} [mm ²]	715	652	360	(94 + 82)*	(94 + 82)*
Number of stacks	3	3	1	4	6
Number of tapes per stack	25	25	21	19	13
Twisting	Reference: yes Non-twisted: no	Yes	No	No	No
I_c (B,T) [kA]	Reference: 14.5 (4 T, 5.6 K) Non-twisted: 13.9 (7 T, 7 K)	14.8 (7 T, 7 K)	10.2 (9 T, 6 K)	A1: 9 (10.9 T, 20 K) A2: 12.2 (10.9 T, 15 K)	12.5 (10.9 T, 20 K)
Number of quench runs	Reference: 9 Non-twisted: 15	18	21	A1: 8 A2: 3	10
Quench conditions # runs × (B, I)	Reference: 8×(3.5 T, 15 kA) 1×(9 T, 9.5 kA) Non-twisted: 13×(6 T, 15 kA) 2×(10.9 T, 11 kA)	16×(6.5 T, 15 kA) 2×(10.9 T, 11 kA)	3×(0 T, 11 kA) 3×(0 T, 15 kA) 3×(6 T, 9 kA) 2×(6 T, 12 kA) 2×(9 T, 9 kA) 2×(9 T, 12 kA) 2×(10.9 T, 9 kA) 3×(10.9 T, 12 kA) 1×(10.9 T, 15 kA)	A1: 6×(7 T, 15 kA) 1×(10.9 T, 12 kA) 1×(10.9 T, 15 kA) A2: 2×(10.9 T, 12 kA) 1×(10.9 T, 15 kA)	7×(7 T, 15 kA) 1×(9 T, 15 kA) 1×(10.9 T, 12 kA) 1×(10.9 T, 13 kA)

*Sum of the aluminum + stainless steel jackets.

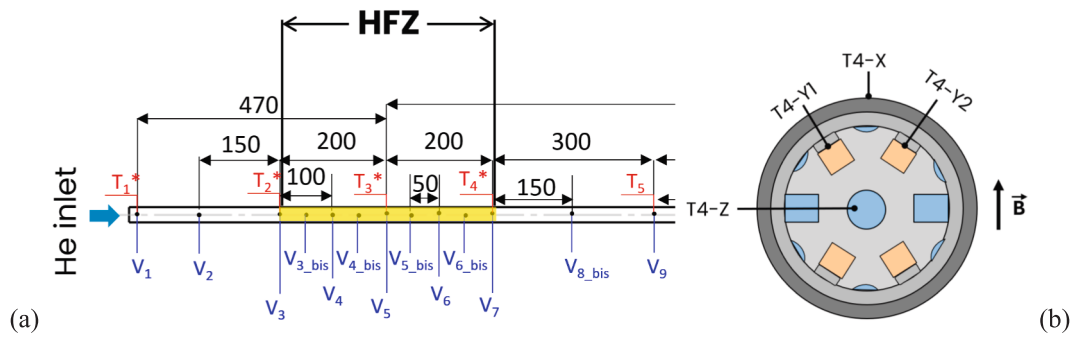


Fig. 1. (a) Schematics of the diagnostics implemented in the A1 conductor in the High Field Zone (HFZ) region: voltage taps placed on the external jacket ($V_{\#}$) and on the slotted-core ($V_{\#,bis}$) are shown. Temperature sensors ($T_{\#}^*$) are arranged as shown in the cross-section in (b); $T_{\#}$ indicates locations where a temperature sensor was placed on the external jacket only. The direction of the background field is also shown.

a twist pitch equal to 400 mm and 1 m, respectively. The triplet is then jacketed in an 8.5-mm-thick stainless steel conduit (grey region in Table 1). The remaining voids between the round strands (light blue region in Table 1) are available for the forced flow helium which is used to cool the conductor or to induce the quench during the Quench Experiment. In the case of the Solder-filled conductor, part of the void space inside the jacket is filled with solder to increase the area of heat transfer between the cable and the jacket (with respect to that of the other two conductors). The ASTRA conductor is made of a single stack of tapes oriented parallel to the background magnetic field. The stack is soldered and placed in a U-shaped copper profile. Unlike the other conductors, the cooling of the stack is indirect, i.e., heat flows through the top and bottom copper bars to reach the segregated helium cooling channel, see the cross-section in Table 1. The ASTRA conductor was the only one equipped also with cartridge heaters (each 25 mm long and 3 mm in diameter) embedded in the jacket to induce the quench, while for all the other conductors it was induced increasing the helium inlet temperature. Concerning the diagnostics of these conductors, voltage is measured on the external jacket with voltage taps placed at a distance of 10 cm in the HFZ. Temperature was measured both on the external jacket as well as with helium-tight sensors protruding through the jacket to measure the temperature of the helium stream. In addition, in ASTRA, temperature sensors were added protruding through the jacket and measuring the temperature close to the copper profile which contains the stack. Further details on the design, diagnostics and measurements performed on the SPC conductors can be found in [7,10] and [11].

3. DC performance evolution

The evolution of the conductor performance after the quench experiment with respect to that before the experiment has been monitored for all the tested conductors. The performance is discussed in terms of critical current, I_C , current sharing temperature, T_{CS} , and their degradation (reduction) after the quench experimental campaign.

During the tests performed on the SPC conductors, the DC performance (I_C and/or T_{CS}) was measured before and after the quench tests [11]. Note that the Reference conductor was found to be degraded (~20 % reduction of the I_C) before starting the actual SULTAN test. To track the DC performance evolution, during the tests of the ENEA conductors (in particular, A1 and B1), a T_{CS} test was performed before each quench test.

Fig. 2 reports the ratio of the critical current at the end of the quench experimental campaign with respect to the pristine sample, plotted as a function of the maximum hotspot temperature reached during the quench test. Note that the maximum hotspot temperature reported in Fig. 2 corresponds to that reconstructed from the voltage measurement, which is closer to the actual maximum temperature reached during quench with respect to the maximum measured temperature, as the latter depends on the quality of the thermal contact of the temperature sensors with the hotspot region. This aspect is further discussed and detailed quantitatively in Section 4.

Focusing on the REBCO SPC conductors (Reference, Non-twisted, Solder-filled and ASTRA), it looks that a correlation between the

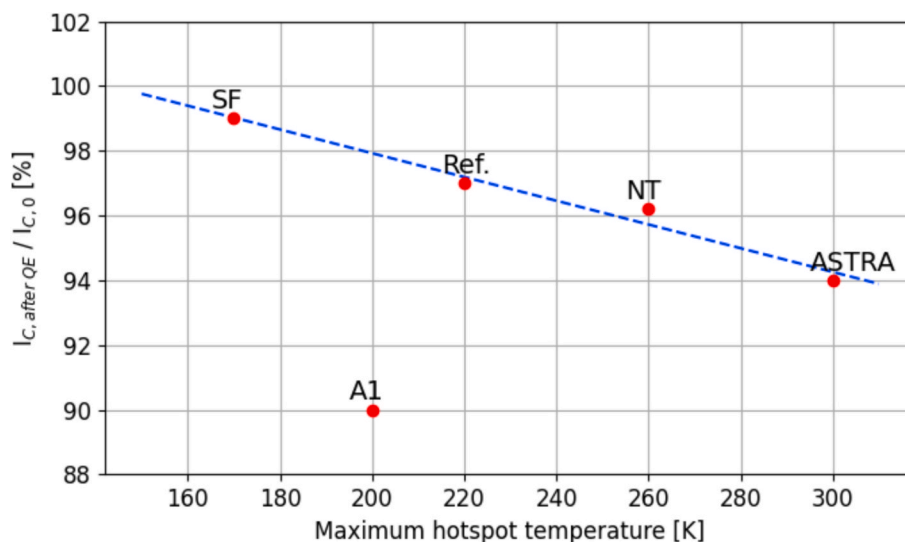


Fig. 2. Ratio of the critical current after -with respect to that before- the quench experiment and the corresponding maximum “virtual” hotspot temperature (reconstructed from the voltage measurement, see Section 4 for the details) reached in the experimental campaign, for each conductor tested.

maximum temperature reached in the test campaign and the amount of degradation is present: the larger the hotspot temperature, the larger the performance degradation.

In terms of I_C reduction, the only reliable point of the ENEA conductors is that of A1, because the results coming from A2 are not clear in their interpretation and the I_C of B1 was measured in different conditions at the end of the test.

Looking at the amount of degradation of each conductor, it is evident that the ENEA conductors degraded more than those designed and manufactured by SPC: ENEA A1 degraded more than, e.g., the Reference conductor, which reached a similar hotspot temperature. The detailed understanding of this degradation mechanism and the motivation of the different quantitative behaviour between the SPC and ENEA conductors would require a thermo-mechanical analysis which is beyond the scope of this work. An integrated platform has been developed and presented in [12], coupling a thermal-hydraulic model, where the actual temperature profile during quench propagation is computed, and a 3D thermo-mechanical model. First results show that the secondary strain induced by the localized thermal expansion in the stack may lead to superconductor performance degradation. In the case of ENEA conductors, the higher coefficient of thermal expansion of the aluminum core with respect to that of the stacks leads to a larger peak strain in the tapes; however, this is partially mitigated by the absence of solder [12], allowing the stack to have a slightly different deformation with respect to the core.

Summing up these results, it looks that these kinds of conductors, i.e., those based on the stacked-tape concept, may safely resist up to a hotspot temperature of roughly 150 K: above this value, they may start degrading.

As mentioned, the conductor performance, in terms of T_{CS} , were measured after each quench test performed in the conductor ENEA A1 and B1. The T_{CS} has been retrieved fitting the data measured by the voltage taps V5-V6 and T3X see Fig. 1(b), with the power law $E = E_0 + E_C(T/T_{CS})^m$, where the electric field E is obtained simply dividing the voltage measurement by the distance between the taps (10 cm), E_0 is a constant offset which includes the systematic offset of the measurement as well as potential resistive contribution, the critical electric field E_C is 1 $\mu\text{V}/\text{cm}$, T is the measured temperature and T_{CS} and m are the fitting parameters.

The systematic measure of the T_{CS} is useful in understanding whether a gradual degradation is caused by each quench or there is a threshold beyond which the performance starts degrading. Fig. 3 shows that the T_{CS} performance of A1 (measured at 15 kA, 10.9 T) is stable until a

hotspot temperature of ~ 135 K is reached. One final quench experiment reaching ~ 200 K was carried out and the performance had clearly degraded, also confirmed by I_C measurements performed after this last quench experiment. The same trend is observed for B1: its T_{CS} (measured at 13 kA, 10.9 T) remained stable within ~ 0.5 K up to a quench with an hotspot temperature of ~ 180 K. After a quench reaching ~ 220 K, the T_{CS} decreased by more than 2.5 K. Additional T_{CS} tests after the last quench showed that it stabilized again in the range 10.5–11 K, confirming that the quench was actually the root cause of that degradation.

The first point in Fig. 3 for A1 reports the T_{CS} measured before the first quench. It is clear that after the first quench, even though the hotspot temperature was quite low (~ 45 K), the T_{CS} decreased noticeably and then it remained stable as discussed previously. A possible explanation of this behaviour is that the first quench may have affected the current redistribution in the bottom joint of the sample, which is close to the HFZ, where the T_{CS} is measured. An alternative explanation is that the first quench may have caused, through a mechanical movement, an adjustment of the tapes in the stacks and/or of the stacks in the slots, as they are not soldered. Therefore, it is advisable, when executing such experiments, to perform at least an additional T_{CS} test after the first quench to quantify this initial variation of T_{CS} . Nevertheless, the focus here is on the impact of increasing hotspot temperatures reached during the quench on the conductor performance, therefore the interest on the variation of the T_{CS} after the first quench with a low hotspot is limited: subsequent quenches (after the first), with increasing hotspot temperatures, show no impact on the conductor performance, thus it is reasonable to assume that the mechanism that caused the initial drop of T_{CS} is different with respect to that causing the last drop of T_{CS} , which instead appears to be related to the hotspot reached during the last quench.

4. Quench analysis

The analysis of the quench experiments is performed according to an analytical model based on the adiabatic assumption to compute the maximum temperature evolution once the quench has started propagating. The method is based on a slightly modified version of that already used in [7] and it is validated against local voltage measurements. This method is historically used to size the stabilizer cross-section in LTS conductors [13]. Then, it is used to assess the performance of a magnet wound with conductors similar to those tested in the experimental campaign. The maximum temperature computed in case of magnet operation is then compared to the 150 K limit introduced in Section 3 to assess which design may perform better and give hints on

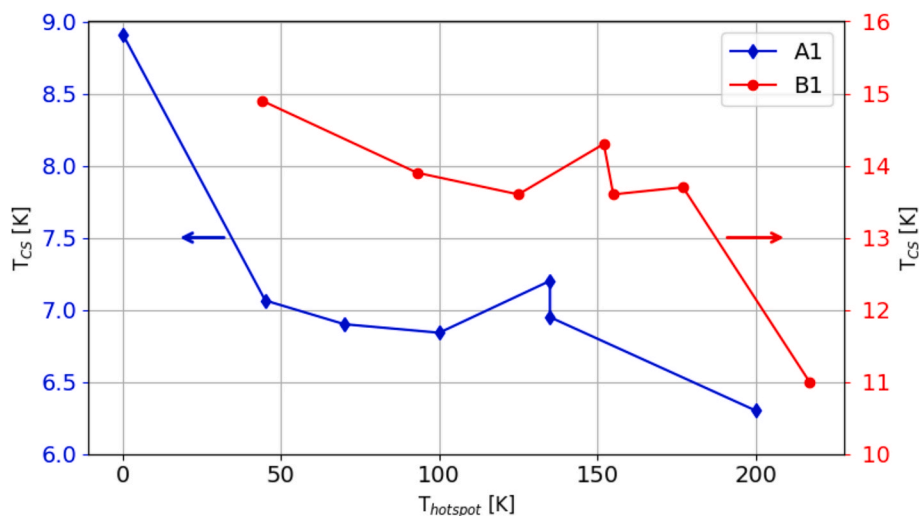


Fig. 3. Evolution of the current sharing temperature T_{CS} in the conductor ENEA A1 and B1 after the value of hotspot temperature reported on the x-axis was reached in a previous quench test.

future design developments in this regard.

Assuming adiabatic quench propagation, the heat balance equation can be written as

$$\int_{T_t}^{T_{max}} \frac{C(T)S}{R'(T)} dT = \int_0^t I(t)^2 dt \quad (1)$$

where the heat capacity $C(T)S$ is defined as $C(T)S = (\rho c_p S)_{stabilizer} + f \cdot (\rho c_p S)_{jacket}$, where ρ is the mass density, c_p is the temperature-dependent specific heat capacity and S is the cross-section, computed for both the stabilizer (copper for the SPC conductors, aluminum for the ENEA conductors), f is a parameter (between 0 and 1) which depends on how much heat capacity of the jacket is available, i.e., thermally coupled, with the stabilizer; $R'(T)$ is the resistance per unit length, computed as $R'(T) = (\rho_{el}(T)/S)_{stabilizer}$, where $\rho_{el}(T)$ is the temperature-dependent electric resistivity of the stabilizer (in case of copper, the dependence on the magnetic field and on the RRR is also taken account) [14], while in the case of the aluminum core of the ENEA conductors the resistivity was directly measured; $I(t)$ is the time-dependent current carried by the conductor (which, in the case of the quench test in SULTAN, was held constant before dumping it); T_t and T_{max} are the so-called transition temperature [15] and maximum temperature reached at each instant t . The transition temperature T_t is not known a priori, although several possible approximations based on the current sharing temperature T_{CS} and critical temperature T_C were proposed. In this case, T_t can be retrieved from the measured quench propagation velocity.

The latter, according to the derivation presented in [15] and used in [7], is defined as

$$QPV = I \sqrt{\frac{R'(T_t) \cdot k(T_t) \cdot S}{C(T_t)S \cdot \int_{T_0}^{T_t} C(T)S dt}} \quad (2)$$

where k is the temperature-dependent thermal conductivity of the stabilizer and T_0 is the operating temperature far away from the normal propagating zone. T_t in the range of 30–45 K are obtained for the conductors analyzed from the QPVs reported in Section 5.

Unlike the approach presented in [7], the maximum temperature considered in Eq. (1) is not the largest measured temperature measured by sensors, but that reconstructed from the voltage measured. The latter gives a more accurate approximation of the actual maximum temperature reached in the quenched region throughout the quench propagation. The reconstructed, also called “virtual”, temperature is derived from the local voltage measured in the high field zone according to

$$V_{HFz}(t) = \rho_{el}(T(t)) \cdot \frac{L}{S} \cdot I \quad (3)$$

where $\rho_{el}(T)$ is the temperature-dependent stabilizer resistivity, L is the distance between the voltage taps (typically 10 cm), S is the stabilizer cross-section. From the experiment, $V_{HFz}(t)$ and I are measured, L and S are known geometrical quantities and the stabilizer resistivity is known as well. Thus, Eq. (3) can be solved for $T(t)$ with an implicit equation solver. The assumptions behind Eq. (3) are mainly that the whole stabilizer is assumed to be at the same temperature and the current is only carried by the stabilizer itself. The first has also been verified experimentally (measuring the temperature as close as possible to the stack and/or its surrounding material, such as copper) and numerically with a 3D model [9], since the stabilizer has a good thermal contact with the stack of tapes and it has a quite good thermal diffusivity, leading to a good homogenization of the temperature across the stabilizer itself. The second assumption implies that the method can be applied above T_t , i.e., when the current is not flowing in the superconductor anymore. On the other hand, in the case of the SPC conductors, having a large steel jacket cross-section, a fraction of the current begins flowing in the jacket as well, however at the maximum temperature it is expected to be around 10 %, thus as a first approximation it can be considered to be flowing

entirely in the stabilizer.

The comparison between the “virtual” temperature computed from Eq. (3) and the actual measured temperature in different conductors is reported in Fig. 4, as a function of $q = \int_0^t I(t)^2 dt$, as q is proportional to the energy deposited during the quench propagation. It is clear that, when the temperature is measured far from the location where the hotspot is expected (i.e., in the copper around the stacks for the SPC conductors or on the stack themselves for the ENEA conductors), a temperature much lower than the “virtual” one is measured. On the other hand, in the case of the ENEA conductors, where the temperature is measured very close to the stacks, see Fig. 1(b) or in the case of the ASTRA conductor, where there is a temperature sensor close to the copper profile around the stack, both the measured and “virtual” temperatures agree quite well. This confirms that the “virtual” temperature gives a reliable assessment of the actual hotspot temperature reached during the experiment.

The amount of heat capacity of the steel jacket actually available during the quench propagation, lumped in the parameter f in Eq. (1), can be derived from the evolution of the maximum temperature. The latter can be either measured (or reconstructed from the measured voltage) or modelled with a simple 2D thermal model. This is a direct consequence of the adiabatic assumption done to derive Eq. (1) itself.

The 2D model solves the transient heat diffusion equation, imposing:

- as thermal driver, the heat deposition due to Joule effect in the stabilizer
- adiabatic boundary conditions on the external boundaries as well as on those at the interface with the helium: this assumption is motivated by the fact that we are interested in the phase of the quench propagation when all the current is already carried by the stabilizer, thus the helium is supposed to be at very low density, thus not impacting the heat transfer on the cross-section.

The evolution of the maximum temperature in the case of the Non-twisted conductor computed for two different cases is reported in Fig. 5(a). One case refers to a perfect thermal contact between the copper and the stainless steel, while the other case refers to a thermal contact interface resistance as measured in [16]. This comparison highlights that the impact of the contact resistance at the interface between copper and stainless steel is negligible. It is worth noting here that the value of the contact resistance should not be compared with that adopted for the 1D modelling of such conductors, see for example [8], because that value accounts mainly for the effect of the shape of the conductor, which cannot be taken into account in the 1D modelling. Here, it is shown that most of the impact on the parameter f is given by the actual geometry of the conductor, i.e., in this case the point contact between the copper and the steel as well as the large value of the steel thickness, with respect to the actual thermal contact resistance. The impact of these features on the temperature distribution in the steel is clearly visible in Fig. 5(b), where the temperature in the steel jacket is far from being uniform.

Fig. 5(a) shows also that the 2D model computes a maximum temperature in good agreement with the experimental data, meaning that this simple modelling approach can be used to follow the thermal evolution once the quench has started its propagation. Furthermore, it is also reported the evolution of the maximum temperature computed with Eq. (1) with $f = 0.12$ and it is worth noting that both the experimental and computed results based on the 2D model would have led to the same value of f .

The 2D modelling approach is especially useful to retrieve f in the case of the ENEA conductors. In this case, the tested conductors were equipped with a thin steel jacket, which was not scaled with respect to the dimensions expected in the actual full size conductor. Therefore, to make a fair comparison between the different conductors in the next section, two different 2D models of the ENEA conductors have been

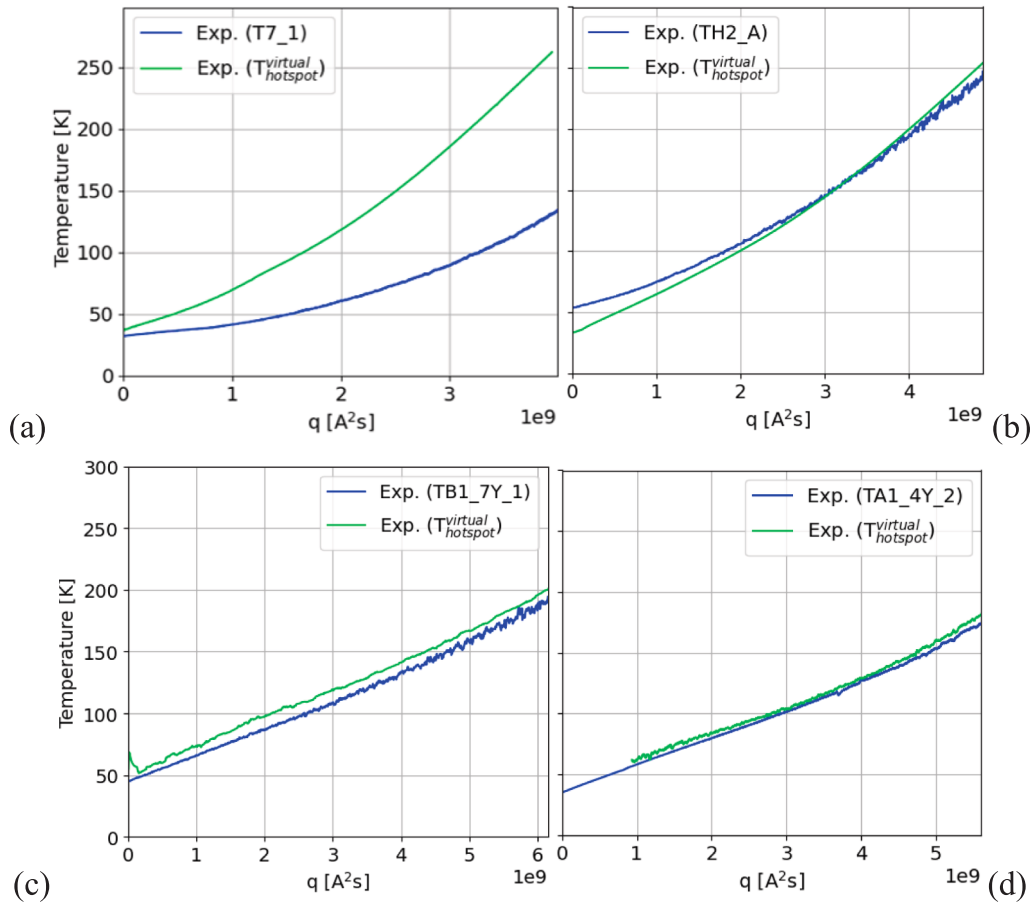


Fig. 4. Comparison of the evolution of the largest measured temperature and the virtual temperature reconstructed from the measured voltage in the Non-twisted (a), ASTRA (b), ENEA B1 (c) and A1 (d) conductors.

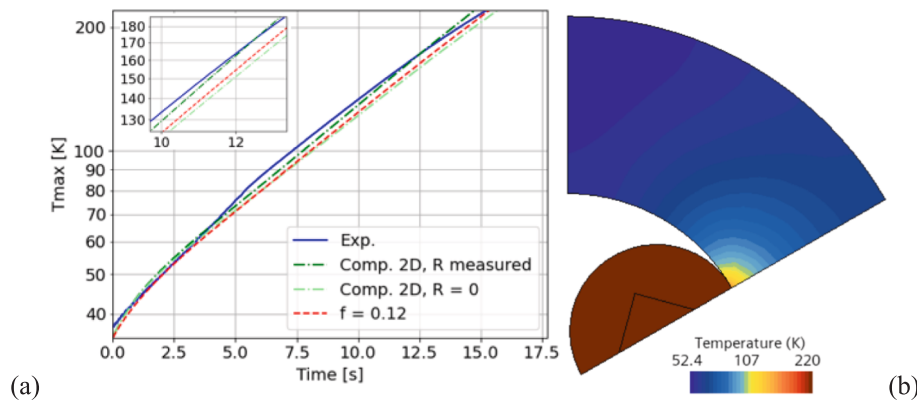


Fig. 5. (a) Evolution of the maximum measured temperature compared to that computed with the 2D model with different thermal contact resistance and that corresponding to $f = 0.12$. (b) Temperature distribution in the 2D model of the Non-twisted conductor when the maximum temperature reaches 220 K.

developed. A first model implements the same geometry of the conductors that were tested. In this way, the reliability of the model results was cross-checked against the experimental data, see Fig. 6(a), leading to a good agreement on the maximum temperature evolution. Next, a second model was developed, this time implementing the conductor geometry with a jacket that is compliant with the expected dimensions of the full size one, i.e., 750 mm², see Fig. 6(b). With this model, the evolution of the maximum temperature was computed and the corresponding f value was retrieved. Also in this case, only a fraction of the entire -thick- jacket actually contributes to the effective heat capacity: as

reported in Fig. 6(c), a value of $f = 0.3$ is suitable for the ENEA conductor if the thick jacket is considered.

The procedure discussed for the Non-twisted conductor was followed also for the other conductors, obtaining an $f = 0.5$ for the Solder-filled conductor, confirming that the larger heat transfer surface between the strands and the jacket increased the fraction of steel participating to the effective heat capacity, and an $f = 0.55$ was obtained for the ASTRA conductor (mainly because the steel cross-section was roughly half of that of the other SPC conductors). The same value of $f = 0.3$ was obtained for the ENEA B1, obtaining the same level of agreement shown in

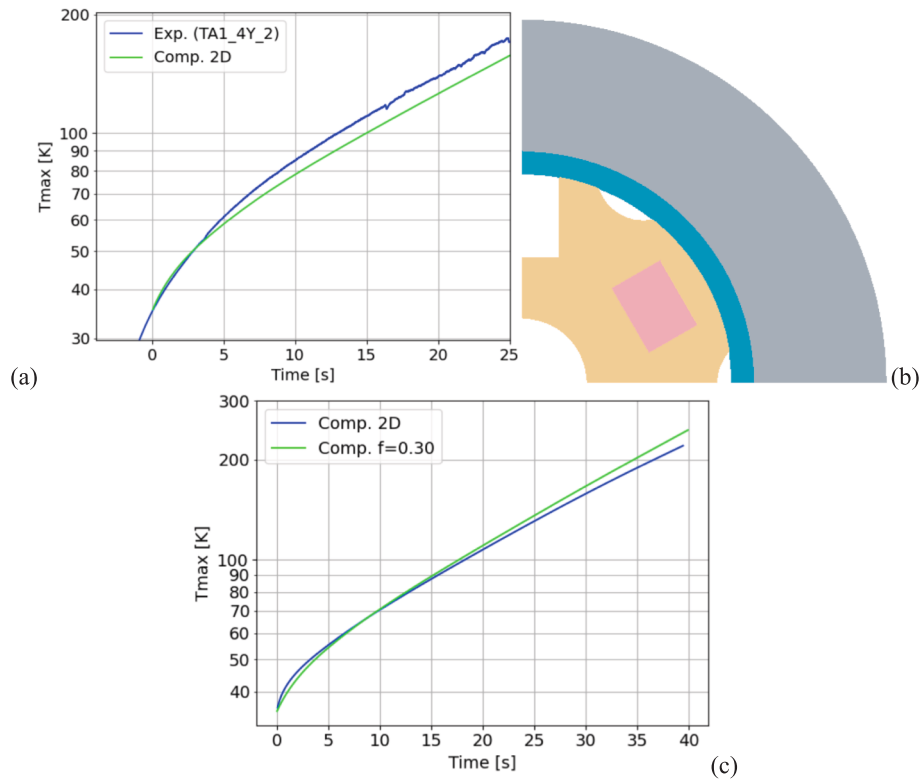


Fig. 6. (a) Evolution of the maximum measured temperature on the ENEA A1 conductor compared to that computed with the 2D model. (b) Geometry of the ENEA A1 2D model accounting for the thicker jacket. (c) Evolution of the maximum temperature computed with the 2D model with the thicker jacket compared to that computed analytically with $f = 0.3$.

Fig. 6 for ENEA A1, as well as the same value obtained for the Non-twisted conductor was found for the Reference conductor, as the twisting of the strands does not have a remarkable impact on the quench propagation.

The performance of the simplified model, made of Eq. (1) and Eq. (3) can be cross-checked against the localized voltage measured in the HFZ during the quench propagation. **Fig. 7** shows that the computed voltage on 10 cm follows closely the measured, thus confirming the reliability of this approach.

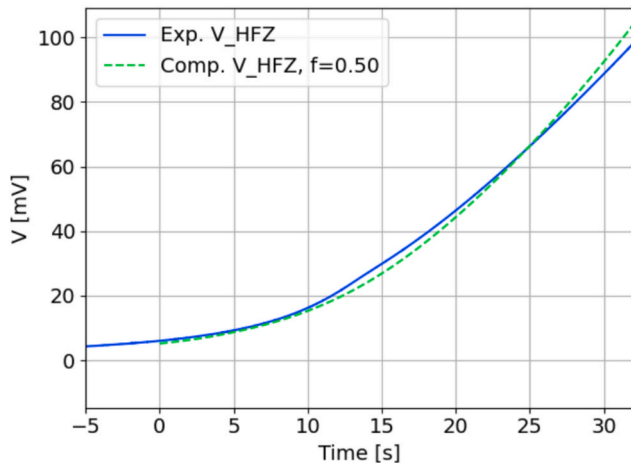


Fig. 7. Comparison of the measured and computed local voltage in the High Field Zone for the Solder-filled conductor.

5. Projection to magnet operation

The magnet of interest considered in this Section is the EU DEMO CS in its hybrid design [17], i.e., equipped with HTS inner layers and LTS in the outermost layers.

The operating conditions are summarized in **Table 2**. The voltage threshold for the quench detection has been set to a conservative value of 500 mV (ITER will use a threshold of 300 mV [18]). A larger value than ITER is considered because EU DEMO conductors will be larger than ITER ones, thus reducing the effectiveness of the ITER-like voltage-based quench detection. Once the quench has been detected, an additional time equal to t_{delay} is considered before starting the exponential dump of the current (following the characteristic current discharge time of $\tau = 15$ s). The conductor cross-sections were simply multiplied by four in order to make them compatible with an operating current of 60 kA and to be consistent with the foreseen discharge time constant $\tau = 15$ s. Note that at the present stage it is not clear what will be the actual conductor design to be adopted in the coil, as other open issues, i.e., performance degradation of the full conductors with electromagnetic cycles, are still to be solved or tested. Nevertheless, the sub-size conductors have been scaled down with respect to the transport current foreseen in the actual coil, therefore scaling up their cross-sections looks

Table 2
Operating conditions of EU DEMO CS relevant for the calculation of the hotspot temperature.

Parameter	Value
B [T]	18
I [kA]	60
τ [s]	15
t_{delay} [s]	1.1
$V_{threshold}$ [mV]	500
T_0 [K]	5

reasonable to estimate their behavior in case of quench during the coil operation.

To assess the voltage rise and, consequently, the hotspot temperature during a quench in the magnet configuration, the relation to be used needs to account for the propagation of the quenched region through the QPV according to

$$V_{total}(t) = 2 \bullet R(T_{max}(t)) \bullet QPV \bullet t \bullet I(t) \tag{4}$$

where $2 \bullet QPV \bullet t$ is the length of the normal zone (being QPV the velocity of a single quench front).

The impact of the magnet operating conditions on parameters computed in the previous Section is mainly on the QPV, because the conductor is expected to operate with a larger temperature margin, i.e., with a smaller ratio of I_{op}/I_C with respect to that in the SULTAN test. However, the conductor is expected to operate at a higher magnetic field (18 T) with respect to that in SULTAN, thus reducing the critical temperature of the superconductor. A larger temperature margin and a lower critical temperature contribute in opposite way on the QPV, thus the value adopted in the following analysis is the same as that computed in Section 4, i.e., those computed from the SULTAN experiment. The only non-negligible variation of QPV is on the ENEA B1 conductor, because it had a larger T_{CS} and it was tested at $T_0 \sim 25$ K. Therefore, considering $T_0 = 5$ K, a decrease of QPV from 24 mm/s to 18 mm/s would be achieved for the ENEA B1 conductor. The QPVs for the other conductors are ~ 58 mm/s for the Reference and Non-twisted, ~ 13 mm/s for the Solder-filled, ~ 34 mm/s for ASTRA and ~ 26 mm/s for ENEA A1 and A2.

The comparison of the voltage and hotspot evolution of the different conductors during quench in magnet operating conditions is shown in Fig. 8(a). The Reference and Non-twisted conductors feature the fastest voltage rise, corresponding to the fastest temperature increase. This

means that the quench is detected first in those kinds of conductors than on the others, thus the dump starts sooner than in the other conductors. However, the hotspot temperature in the Reference and Non-twisted conductors raises more than all the others. This is due to the smaller effective heat capacity available during quench propagation. Therefore, the fact that the quench is detected earlier does not compensate the temperature rise with respect to conductors with larger heat capacity.

The other SPC layouts confirm this trend: the ASTRA conductor has a coupling coefficient (f) between the copper and surrounding jacket comparable to that of the Solder-Filled, however, the former features half of the stainless-steel cross-section. This leads to an effective heat capacity of ASTRA that is 30 % larger than the Reference and Non-twisted, whereas it is 34 % smaller than that of the Solder-Filled. The results reported in Fig. 8(b) are coherent with the trend of the effective heat capacity: the maximum temperature reached after the same energy is deposited is the largest for Reference and Non-twisted, intermediate for ASTRA and the lowest for the Solder-filled. However, as the quench detection in ASTRA occurs earlier with respect to the others (except for the Reference and Non-twisted conductors), the final hotspot reached is comparable to the Solder-filled one, see Fig. 8(c).

Concerning the ENEA conductors, in the magnet configuration they behave coherently in terms of voltage considering their QPVs: ENEA B1 has a smaller QPV with respect to ENEA A1, thus, although having a similar geometry, voltage in ENEA B1 raises slower than in ENEA A1, detection occurs later and the final hotspot is larger.

Fig. 8(c) shows that for all the conductors the detection occurs above 100 K. Therefore, considering that the current is exponentially dumped with a time constant of 15 s, there is still a non-negligible amount of energy that is deposited during the current dump. The consequence is that all conductors overcome 200 K as hotspot and the Reference and Non-twisted go beyond 300 K. This means that the current design and quench detection schemes are such that the criterion identified in

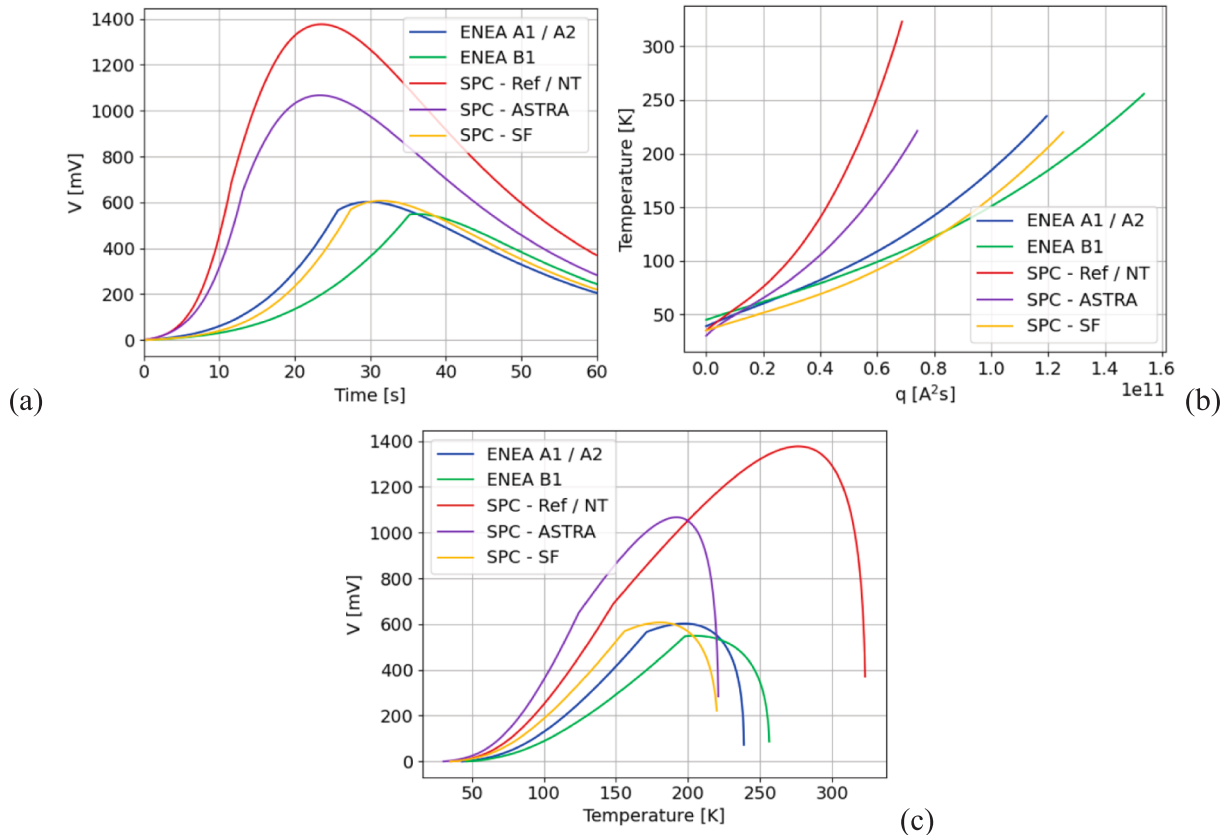


Fig. 8. Evolution of the (a) voltage and (b) hotspot temperature for the different conductor layouts proposed in magnet configuration. (c) Evolution of the voltage as function of the hotspot temperature.

Section 3, i.e., to stay below 150 K, is not fulfilled. Therefore, improvements and/or alternative solutions for those aspects should be pursued.

From the conductor design point of view, the results show that it is better having a conductor with a large *effective* heat capacity. The most convenient way to obtain the latter is to improve the thermal contact between the copper and stainless-steel, without increasing the conductor cross-section. Nevertheless, these conductors exhibit large solid (conductive) cross-sectional area, thus leading to possibly large AC losses in pulsed magnets with respect to low temperature superconductors. To counteract this disadvantage, a solution has already been proposed by different designers [19,20], consisting in sectorizing the bulky conductive cross-section in order to reduce the effective area available for eddy currents. Preliminary electro-magnetic tests have shown promising results, although improvements in the heat removal capabilities of such bulky conductors could be needed. Furthermore, as discussed in [21], the field ramp rates expected in the EU DEMO CS are such that coupling losses are not the primary loss mechanism when compared to hysteresis losses, thus larger conductive cross-sections would not increase much the total AC losses.

From the quench detection point of view, several alternative strategies are being investigated, such as fiber optics [22], superconducting quench detection wires [7] and thermocouple chains [23], which showed, having been tested in SULTAN, a faster quench detection with respect to voltage measurement.

6. Conclusions and perspective

The Quench Experiment campaign supported by EUROfusion has allowed to successfully test seven REBCO conductors based on different conductor layouts. The analysis of the evolution of the DC performance before, during and after the experimental campaign shows that a temperature peak above 150 K may lead to DC performance degradation. This provides a first reference value that conductor designers may refer to, impacting both the magnet quench detection strategy as well as the conductor design itself.

The projection to the actual magnet operating conditions confirmed that the effect of a larger effective heat capacity is beneficial, as it leads to a lower hotspot temperature. However, this may pose a challenge in designing a conductor with larger effective heat capacity, but suitable with the pulsed operations where it is foreseen to be employed. Also, improvements in the quench detection, that would be beneficial in reducing the hotspot temperature, are encouraged, as the current combination of conductor design and magnet operating conditions would lead to too large hotspot temperature with respect to the 150 K threshold quantified after the quench experiments.

The experimental campaign is still ongoing and other layouts manufactured by other EUROfusion research units are planned to be tested, thus enriching the experimental database on the quench behavior in HTS conductors.

CRediT authorship contribution statement

A. Zappatore: Writing – original draft, Visualization, Methodology, Formal analysis. **H. Bajas:** Writing – review & editing, Investigation, Data curation. **N. Bykovskiy:** Writing – review & editing, Methodology, Investigation, Data curation. **P. Bruzzone:** Resources, Conceptualization. **G. Celentano:** Writing – review & editing, Methodology, Investigation, Formal analysis, Conceptualization. **G. Colombo:** Writing – review & editing, Investigation, Formal analysis. **J. Greenwood:** Writing – review & editing, Investigation, Data curation. **A. Masi:** Writing – review & editing, Investigation. **K. Sedlak:** Writing – review & editing, Resources, Conceptualization. **D. Uglietti:** Writing – review & editing, Investigation, Formal analysis. **V. Corato:** Writing – review & editing, Supervision, Project administration, Methodology, Funding acquisition, Conceptualization.

Declaration of competing interest

The authors declare the following financial interests/personal relationships which may be considered as potential competing interests: Valentina Corato reports financial support was provided by European Consortium for the Development of Fusion Energy. If there are other authors, they declare that they have no known competing financial interests or personal relationships that could have appeared to influence the work reported in this paper.

Acknowledgements

This work has been carried out within the framework of the EUROfusion Consortium, funded by the European Union via the Euratom Research and Training Programme (Grant Agreement No. 101052200—EUROfusion). Views and opinions expressed are however those of the author(s) only and do not necessarily reflect those of the European Union or the European Commission. Neither the European Union nor the European Commission can be held responsible for them.

Data availability

Data will be made available on request.

References

- [1] Uglietti D, Bykovskiy N, Sedlak K, Stepanov B, Wesche R, Bruzzone P. Test of 60 kA coated conductor cable prototypes for fusion magnets. *Supercond Sci Technol* 2015;28:124005.
- [2] Celentano G, de Marzi G, Fabbri F, Muzzi L, Tomassetti G, Anemona A, et al. Design of an industrially feasible twisted-stack HTS cable-in-conduit conductor for fusion application. *IEEE Trans Appl Supercond* 2014;24:1–5.
- [3] Hartwig ZS, et al. VIPER: an industrially scalable high-current high-temperature superconductor cable. *Supercond Sci Technol* 33; 2020: 11LT01.
- [4] Mulder T, van der Laan D, Weiss JD, Dudarev A, Dhallé M, ten Kate HHJ. Design and preparation of two REBCO-CORC cable-in-conduit conductors for fusion and detector magnets. *IOP Conf Ser: Mater Sci Eng* 2017;279 012033.
- [5] Hartwig ZS, et al. The SPARC toroidal field model coil program. *IEEE Trans Appl Supercond* 2024;34(2):0600316.
- [6] Corato V, et al. Strategy for developing the EU-DEMO magnet system in the concept design phase. *IEEE Trans Appl Supercond* 2022;32:1.
- [7] Bykovskiy N, Bajas H, Dicuonzo O, Bruzzone P, Sedlak K. Experimental study of stability, quench propagation and detection methods on 15 kA sub-scale HTS fusion conductors in SULTAN. *Supercond Sci Technol* 2023;36:034002.
- [8] Zappatore A, Bonifetto R, Bruzzone P, Corato V, Dicuonzo O, Kumar M, et al. Quench experiments on sub-size HTS cable-in-conduit conductors for fusion applications: data analysis and model validation. *Cryogenics* 2023;132:103695.
- [9] Zappatore A. Full 3D thermal-hydraulic and electric modelling of quench propagation in HTS conductors. *Supercond Sci Technol* 2024;37:125012.
- [10] Dicuonzo O, Kang R, Sedlak K, Stepanov B, Uglietti D, Wesche R, et al. Upgrade and commissioning of the SULTAN facility to host quench experiments on HTS high current conductors. *IEEE Trans Appl Supercond* 2021;31:9500505.
- [11] Dicuonzo O. Electromechanical investigations and quench experiments on sub-size HTS cables for high field EU-DEMO central solenoid PhD Thesis (EPFL); 2022 (available at: <http://infoscience.epfl.ch/record/293510>).
- [12] De Bastiani M, Bonifetto R, Boso DP, Corato V, Zanino R, Zappatore A. Development of an integrated thermo-mechanical simulation environment for quench analyses in HTS cables for fusion. *IEEE Trans Appl Supercond* 2024;35(5):4600205.
- [13] Kovari M, Fox F, Harrington C, Kembleton R, Knight P, Lux H and Morris J. “PROCESS”: A systems code for fusion power plants – Part 2: Engineering Fusion Engineering and Design 2016; 104: 9-20.
- [14] Drexler ES, Reed RP, Simon NJ. Properties of copper and copper alloys at cryogenic temperatures (Washington DC: NIST Monograph 177, U.S. Government Printing Office); 1992.
- [15] Iwasa Y. *Case studies in superconducting magnets design and operational issues* 2nd edition. Springer; 2009.
- [16] Weiss K-P, et al. Mechanical and thermal properties of central former material for high-current superconducting cables in IEEE Transactions on Applied Superconductivity 2016; 26(4): 8800604.
- [17] Wesche R, et al. Hybrid HTS-Nb3Sn-NbTi DEMO CS coil design optimized for maximum magnetic flux generation. *Fusion Eng Des* 2018;146:10–3.
- [18] Coatanea M, Duchateau JL, Hertout P, Bessette D, Rodriguez-Mateos F. Quench Detection in the ITER Magnet System IEEE Transactions on Applied Superconductivity 2010; 20(3).
- [19] Muzzi L, et al. Design and feasibility assessment of an HTS sector shaped high-current conductor for fusion coils. *IEEE Trans Appl Supercond* 2023;33(5):4200106.

- [20] Sanabria C, et al. Development of a high current density, high temperature superconducting cable for pulsed magnets. *Supercond Sci Technol* 2024;37:115010.
- [21] Uglietti D, Kang R, Wesche R, Grilli F. Non-twisted stacks of coated conductors for magnets: analysis of inductance and AC losses. *Cryogenics* 2020;110:103118.
- [22] Salazar E, et al. Fiber optic quench detection for large-scale HTS magnets demonstrated on VIPER cable during high-fidelity testing at the SULTAN facility. *Supercond Sci Technol* 2021;34:035027.
- [23] Bykovsky N, et al. Temperature-based quench detection methods via integrated superconducting wires and thermocouple chains, presented at IDSM workshop (available at: https://agenda.infn.it/event/32061/contributions/193784/attachments/104732/148261/IDSM_wire-based_QD_Bykovskiy.pdf); 2023.